Contents lists available at ScienceDirect

Physics Letters B

K⁻ absorption on two nucleons and ppK⁻ bound state search in the Σ⁰p final state

O. Vázquez Doce [a,b,*], L. Fabbietti [a,b], M. Cargnelli [c], C. Curceanu [d], J. Marton [c], K. Piscicchia [d,e], A. Scordo [d], D. Sirghi [d], I. Tucakovic [d], S. Wycech [f], J. Zmeskal [c], A. Anastasi [d,g], F. Curciarello [g,h,i], E. Czerwinski [j], W. Krzemien [f], G. Mandaglio [g,k], M. Martini [d,l], P. Moskal [j], V. Patera [m,n], E. Pérez del Rio [d], M. Silarski [d]

[a] Excellence Cluster 'Origin and Structure of the Universe', 85748 Garching, Germany
[b] Physik Department E12, Technische Universität München, 85748 Garching, Germany
[c] Stefan-Meyer-Institut für Subatomare Physik, 1090 Wien, Austria
[d] INFN, Laboratori Nazionali di Frascati, 00044 Frascati, Italy
[e] Museo Storico della Fisica e Centro Studi e Ricerche Enrico Fermi, Italy
[f] National Centre for Nuclear Research, 00681 Warsaw, Poland
[g] Dipartimento M.I.F.T. dell'Università di Messina, 98166 Messina, Italy
[h] Novosibirsk State University, 630090 Novosibirsk, Russia
[i] INFN Sezione Catania, 95129 Catania, Italy
[j] Institute of Physics, Jagiellonian University, 30-059 Cracow, Poland
[k] INFN Gruppo collegato di Messina, 98166 Messina, Italy
[l] Dipartimento di Scienze e Tecnologie applicate, Università 'Guglielmo Marconi', 00193 Roma, Italy
[m] Dipartimento di Scienze di Base e Applicate per l'Ingegneria, Università 'Sapienza', 00161 Roma, Italy
[n] INFN Sezione di Roma, 00185 Roma, Italy

ARTICLE INFO

ABSTRACT

We report the measurement of K⁻ absorption processes in the Σ⁰p final state and the first exclusive measurement of the two nucleon absorption (2NA) with the KLOE detector. The 2NA process without further interactions is found to be 9% of the sum of all other contributing processes, including absorption on three and more nucleons or 2NA followed by final state interactions with the residual nucleons. We also determine the possible contribution of the ppK⁻ bound state to the Σ⁰p final state. The yield of ppK^-/K^-_{stop} is found to be $(0.044 \pm 0.009\,stat^{+0.004}_{-0.005}\,syst) \cdot 10^{-2}$ but its statistical significance based on an F-test is only 1σ.

1. Introduction

The study of the K̄-nucleus interaction at low energies is of interest not only for quantifying the meson–baryon potential with strange content [1], but also because of its impact on models describing the structure of neutron stars (NS) [2]. The K̄-nucleus potential is attractive, as theory predicts [3] and kaonic atoms confirm [4], and this fact leads to the formulation of hypotheses about antikaon condensates inside the dense interior of neutron stars. Although recently measured heavy NS [5] constrain the equation of state of the latter as being rather stiff and hence degrees of freedom other than neutrons are disfavoured and theoretical calculations about nuclear systems with high multiplicity of antikaons present upper limits that disfavour the appearance of a condensate [6], experimental studies of the antikaon behaviour in nuclear matter are needed. The study of antikaons production in heavy-ion reactions at moderate energies ($E_{KIN} \approx$ GeV), with maximal reached baryon densities of $\rho \approx (3\text{–}4) \cdot \rho_0$ (with ρ_0 being the normal nuclear matter density) was carried out to find evidence of a strong attractive potential between antikaons within dense nuclear matter [7]. However, the statistics collected so far [8] does not allow for any conclusive statement about the role played by kaons within dense nuclear matter. In this context it is crucial that the theoretical models used to interpret the data properly include both the rather large cross-sections for antikaon absorption processes on nucleons and the presence of the $\Lambda(1405)$ resonance [1].

* Corresponding author.
E-mail address: oton.vazquez.doce@cern.ch (O. Vázquez Doce).

Indeed, an antikaon produced within nuclear matter can undergo absorption upon one or more nucleons and the measurement of such processes is not yet exhaustive, even at normal nuclear densities [9,10]. Absorption processes also play an important role in the understanding of kaonic atoms, where a substantial multi-nucleon component is put forward by some theoretical models [11]. The $\Lambda(1405)$ link to the antikaon–nucleon interaction resides in the fact that theory describes this resonance as generated dynamically from the coupling of the $\bar{K}$–N and the Σ–π channels [12]. Hence the $\Lambda(1405)$ can be seen, at least partially, as a $\bar{K}$–N bound state. Despite of several experimental measurements [13], not even the vacuum properties of the $\Lambda(1405)$ are yet pinned down precisely and those can also be modified at finite baryonic densities, with major implications for the $\bar{K}$ dynamics in the medium.

Following the line of thought employed to interpret the $\Lambda(1405)$, one or more nucleons could be kept together by the strong attractive interaction between antikaons and nucleons, and then so-called kaonic bound states as ppK$^-$ or ppnK$^-$ might be formed. The observation of such states and the measurement of their binding energies and widths would provide a quantitative measurement of the $\bar{K}$-nucleon interaction in vacuum, providing an important reference for the investigation of the in-medium properties of $\bar{K}$. For the di-baryonic kaonic bound state ppK$^-$, theoretical predictions deliver a wide range of binding energies and widths [14] and experimental results are contradictory [15]. For the search of such states in K$^-$-absorption experiments, the competing multi-nucleonic absorption plays a fundamental role.

This work focuses on the analysis of the Σ^0p final state produced in absorption processes of K$^-$ on two or more nucleons and the search for a signature of the $ppK^- \to \Sigma^0 + p$ kaonic bound state. The chosen Σ^0p final state is free from the ambiguities present in the analysis of the Λp state considered in previous works [10]. Moreover, this study represents the first attempt of combining a quantitative understanding of the absorption processes and contributing background sources with the test of different hypotheses for the ppK$^-$ bound state properties.

2. Σ^0p selection and interpretation

The analysed data corresponds to a total integrated luminosity of 1.74 fb^{-1} collected in 2004–2005 with the KLOE detector [16] located at the DAΦNE e$^+$e$^-$ collider [17]. There, ϕ mesons are produced nearly at rest, providing an almost monochromatic source of K$^-$ with a momentum of $\sim$ 127 MeV/c.

The data here presented was taken by the KLOE Collaboration and provided to the authors for an independent analysis. The KLOE detector consists of a large acceptance cylindrical drift chamber (DC) of 3 m length and 2 m radius surrounded by an electromagnetic calorimeter (EMC) inside an axial magnetic field of 0.52 T. The DC provides a spatial resolution of 150 μm and 2 mm in the radial and longitudinal coordinates, respectively, and a transverse momentum resolution of $\sigma_{p_T}/p_T \sim 0.4\%$ for large angle tracks. The EMC is composed of barrel and end-cap modules covering 98% of the solid angle with energy and time resolutions of $\sigma_E/E = 5.7\%/\sqrt{E(\text{GeV})}$ and $\sigma_t = 54$ ps$/\sqrt{E(\text{GeV})}$, respectively. The DC entrance wall is composed of 750 μm carbon fibre with inner and outer layers of aluminium of 100 μm thickness. The number of stopped K$^-$ in this wall is calculated by combining the experimental K$^+$ tagging efficiency, the luminosity information and a Monte Carlo simulation to determine the rate of K$^-$ stopped in the DC wall. The decay nearly at rest of the ϕ meson allows to tag K$^-$ events by the identification of a K$^+$ track in the opposite hemisphere of the DC. The extracted total number of stopped K$^-$ is equal to $(3.25 \pm 0.06) \cdot 10^8$. This value is used to normalise the measured yields of the different absorption processes. Both in
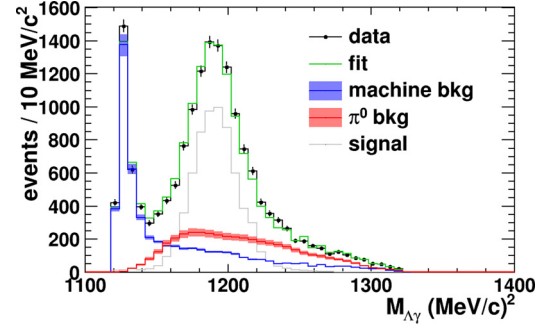

Fig. 1. (Colour online.) $\Lambda\gamma$ invariant mass distribution. The black symbols represent the experimental data, the blue and the red histograms are the contribution from the machine background and events that contain a $\Lambda\pi^0$p in the final state, respectively. The gray histogram shows the simulated Σ^0 signal and the green one the overall fit to the data (see text for details).

flight and at rest K$^-$ absorptions can occur and a weight of 50% is assigned to each process for the normalisation.

The starting point for the selection of K$^-$ absorption processes leading to Σ^0p final state is the identification of a $\Lambda(1116)$ hyperon through its decay into protons and negative pions (BR = 63.8%). Proton and pion track candidates are selected via dE/dx measurement in the DC. For each proton and pion candidate a minimum track length of at least 30 and 50 cm is required, respectively. The track length must also be larger than 50% of the expected length value calculated by extrapolating the measured momentum at the DC entrance. Additionally, proton candidates must have a momentum higher than 170 MeV/c. These selections aim to improve the purity of the particle identification, minimise the pion contamination in the proton sample and minimise the contribution from low momentum tracks that are emitted parallel to the DC wires and reach the EMC barrel. The reconstructed $M_{p\pi^-}$ invariant mass shows a mean value of 1115.753 ± 0.002 MeV/c^2 for the mass, with a resolution of $\sigma = 0.5$ MeV/c^2, well in agreement with the PDG value [18]. The Λ candidates are selected using the following cut: $1112 < M_{p\pi^-} < 1118$ MeV/c^2.

A common vertex between the Λ candidate and an additional proton track is then searched for. The obtained resolution on the radial coordinate ($\rho_{\Lambda p}$) for the Λp vertex is 12 mm, and this topological variable is used to select the K$^-$ absorption processes inside the DC wall. The contamination of events of absorptions in the gas volume of the DC is below 1%. The Λp invariant mass resolution is evaluated with a phase space Monte Carlo simulation where the proton and Λ momenta are varied from 100 to 700 MeV/c and is found to be equal to 1.1 MeV/c^2. The contamination to the proton sample for the Λp final state due to heavier particles (deuterons or tritons) is estimated to be less than 2% by MC simulations of absorption events with Λd and Λt final state.

The Σ^0 candidates are identified through their decay into $\Lambda\gamma$ pairs. After the reconstruction of a Λp pair, the photon selection is carried out via its identification in the EMC. Photon candidates are selected by applying a cut on the difference between the EMC time measurement and the expected time of arrival of the photon within $-1.2 < \Delta t < 1.8$ ns. The resulting $\Lambda\gamma$ invariant mass distribution is shown in Fig. 1, where the Σ^0 signal is visible above a background distribution.

The following kinematic distributions are considered simultaneously in a global fit to extract the contributions of the different absorption processes: the Σ^0p invariant mass, the relative angle of the Σ^0 and proton in the laboratory system $\cos(\theta_{\Sigma^0 p})$, the Σ^0 and the proton momenta. The processes that are taken into account in the fit of the experimental data are:

1. $K^- A \to \Sigma^0\text{-}(\pi)\ p_{\text{spec}}$ (A'),
2. $K^- pp \to \Sigma^0\text{-}p$ (2NA),
3. $K^- ppn \to \Sigma^0\text{-}p\text{-}n$ (3NA),
4. $K^- ppnn \to \Sigma^0\text{-}p\text{-}n\text{-}n$ (4NA).

This list includes the K^- absorption on two nucleons with and without final state interaction for the $\Sigma^0 p$ state and processes involving more than two nucleons in the initial state. These contributions are either extracted from experimental data samples or modelled via simulations and digitised. Nevertheless, the background contributions must be determined and subtracted prior to the global fit.

Two kinds of background contribute to the analysed $\Sigma^0 p$ final state: the machine background and the events with $\Lambda \pi^0 p$ in the final state. Both are quantified using experimental data. The machine background originates from spurious hits in the EMC that enter the photon time coincidence window. It is emulated by a side band analysis, selecting events with EMC hits outside the coincidence window ($-4 < \Delta t < -2$ ns and $3 < \Delta t < 8.2$ ns). The $\Lambda \pi^0 p$ background originates either from a single nucleon absorption followed by the creation of a $\Lambda \pi^0$ or a $\Sigma^0 \pi^0$ pair. In the first case also a rescattering of the Λ/π^0 with one or several of the spectator nucleons could occur while in second case the Σ^0 hypeon undergoes an internal conversion process on a residual nucleon ($\Sigma N \to \Lambda N$) leading to a $\Lambda \pi^0 p$ final state. Events with two photon candidates within the selected time window and with a $\gamma\gamma$ invariant mass around the π^0 nominal mass (3σ of the experimental resolution of 17 MeV/c^2) are selected to emulate the $\Lambda \pi^0 p$ background. Both experimental samples are used together with a simulation of the Σ^0 signal to fit the Λ-photon invariant mass distribution in order to extract the machine and $\Lambda \pi^0 p$ background contributions. Events originating from the $\Sigma^0 \pi^0$ production after a single nucleon absorption followed by the emission of a proton via the final state interaction of the Σ^0 or π^0 contribute to the low energy part of our spectra with a contamination of $3 \pm 2\%$. Full scale simulations of the Σ^0 reconstruction in the $\Lambda\gamma$ channel lead to a mass mean value and σ of 1189 and 14.5 MeV/c^2, respectively. The mean value is slightly shifted with respect to the Σ^0 nominal mass reported in [18] because of the small bias introduced by the reconstruction. This simulation is used to fit the Σ^0 signal on the $\Lambda\gamma$ distribution shown in Fig. 1.

Fig. 1 shows the results of the fit to the $\Lambda\gamma$ invariant mass, with the background and signal components. The black symbols refer to the experimental data, the blue histogram to the fitted machine background, the red histogram to the $\Lambda \pi^0 p$ background, the gray one to the simulated Σ^0 signal and the green histogram to the sum of all fit contributions. The errors shown for the background distributions represent the statistical errors of the fit. To enhance the purity of the experimental data for the following analysis steps, a cut on the $\Lambda\gamma$ invariant mass around the nominal Σ^0 mass is applied. The applied cut, $1150 < M_{\Lambda\gamma} < 1235$ MeV/c^2, corresponds to 3σ of the experimental resolution, and is verified with MC simulation. The contribution of the machine and $\Lambda \pi^0 p$ backgrounds within the selected $\Lambda\gamma$ invariant mass is $(14.6 \pm 0.8)\%$ and $(26.1 \pm 2.7)\%$, respectively. The machine background is directly subtracted from the experimental data for each kinematic distributions used for the global fit. The fit error is added to the statistical errors of the experimental data after the background subtraction. The $\Lambda \pi^0 p$ background is considered in the global fit using the obtained yield as a starting value.

3. Determination of the absorption processes

The cocktail of processes considered for the global fit is obtained as follows. Process 1 corresponds to the uncorrelated production of a proton from the fragmentation of the residual nucleus together with a Σ^0 production from the K^- absorption. This contribution is obtained from experimental data containing Λ–triton–proton, Λ–deuteron–proton or Λ–proton–proton in the final state to emulate the case where the selected proton is barely correlated with the Λ.

For the simulation of the absorption processes 2–4 a ^{12}C target is considered. The Fermi momentum of the interacting nucleons inside the ^{12}C, the initial momentum of the absorbed K^- and the mass difference between the initial and residual nuclei are used in the calculation of the event kinematic. The Fermi momentum distribution of the nucleons in ^{27}Al target is only 9% higher in comparison with ^{12}C. The mass difference of the initial and residual nuclei varies only by 0.3% when considering ^{27}Al in comparison with ^{12}C and this value is lower than the experimental resolution of the $\Sigma^0 p$ invariant mass. For all the considered reactions, the emitted nucleons are required to have a total momentum above the ^{12}C Fermi momentum to be able to leave the nucleus.

For the 2NA (process 2), two cases are studied. One including the final state interaction (2NA-FSI) of the Σ^0 or proton with the residual nucleus, and the second assuming no FSI at all (2NA-QF). In the case of the FSI-free production of the $\Sigma^0 p$ pair, only the fragmentation of the residual nucleus is considered. The following cases for the fragmentation for the spectator nucleus have been considered in the simulations: $K^- + {}^{12}\text{C} \to \Sigma^0 p ({}^{10}\text{Be},\ {}^4\text{He} + {}^4\text{He} + 2n,\ {}^4\text{He} + 2p + 4n,\ 4p + 6n)$. The relative amplitudes of these contributions are left free in the global fit and they are clearly visible in the $\Sigma^0 p$ invariant mass distribution as a low mass tail. All other kinematic variables stay unaffected by the fragmentation process. The FSI for the Σ^0 and p is implemented by allowing the outgoing proton or Σ^0 to scatter elastically with the residual nucleons. The nucleon momentum is sampled according to the Fermi distribution and the scattering probability is assumed to be equal to 50% for both the cases of one and two collisions. The modified kinematic variables of the Σ^0 or proton are then considered in the simulated events used in the global fit. A more sophisticated propagation of the hit probability was investigated [19], but the results show no major differences in the resulting kinematic distributions. This motivates the simplification. Reactions resulting into a $\Sigma^0 n$ final state followed by a rescattering np $\to$ np have also investigated. They result in the same kinematic distributions mentioned above modulus the small n-p mass difference.

The processes 1–4 together with the $\Lambda \pi^0 p$ background sample are used for the global fit. The starting value for the $\Lambda \pi^0 p$ yield is extracted from the fit to the $\Lambda\gamma$ invariant mass but this component is free to vary within 2σ in the global fit. Panels (a)–(d) in Fig. 2 show the experimental distributions for the $\Sigma^0 p$ invariant mass, the $\cos(\theta_{\Sigma^0 p})$, and the Σ^0 and proton momenta, together with the fit results. The black points represent the experimental data after the subtraction of the machine background with the systematic errors shown by boxes. The gray filled histogram represents the $\Lambda \pi^0 p$ background. The cyan distributions show the sum of the 4NA simulation together with the uncorrelated production of the $\Sigma^0 p$ final state. The blue distribution represents the 3NA and the magenta histogram the 2NA-FSI. The red distribution shows the 2NA-QF. The gray line is the resulting total fit. For each fitted distribution the light error band corresponds to the statistical error resulting from the fit, while the darker band visualises the symmetrised systematic error.

The systematic errors for the experimental and simulated distributions are obtained by varying the minimum momentum required for the proton track selection, the time window for the selection of signal and machine background, the yields of the machine background distributions and the selection of the Σ^0 mass.
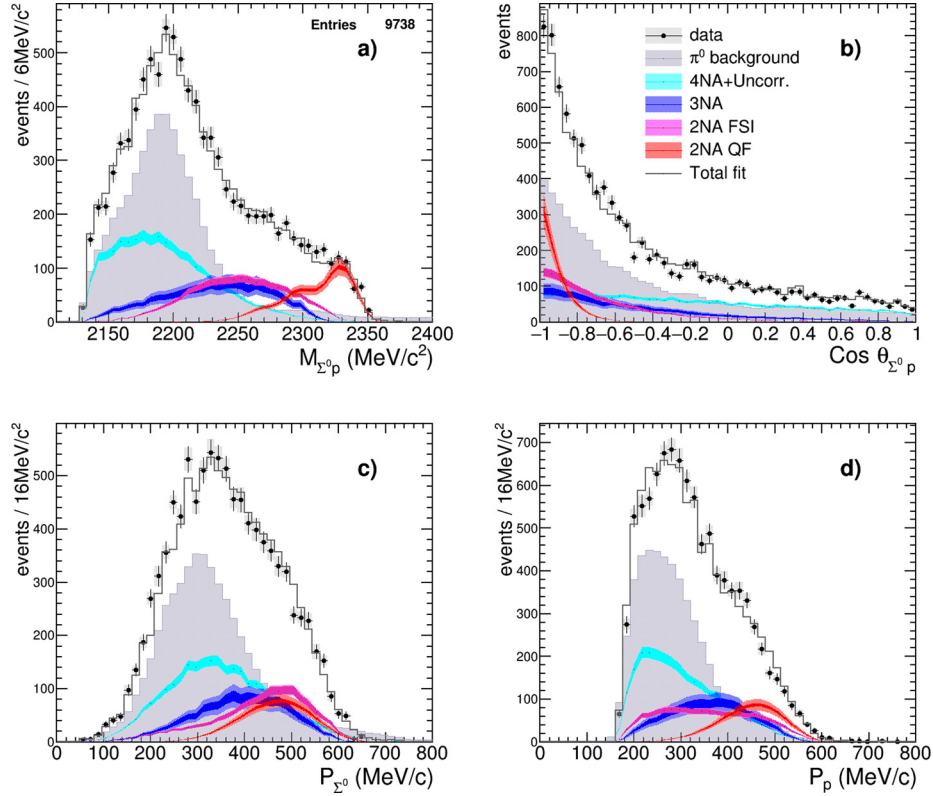
Fig. 2. (Colour online.) Experimental distributions of the $\Sigma^0 p$ invariant mass, $\cos(\theta_{\Sigma^0 p})$, Σ^0 momentum and proton momentum together with the results of the global fit. The experimental data after the subtraction of the machine background are shown by the black circles, the systematic errors are represented by the boxes and the coloured histograms correspond to the fitted signal distributions where the light-coloured bands show the fit errors and the darker bands represent the symmetrised systematic errors. The gray line shows the total fit distributions (see text for details).

The obtained resolution for the $\Lambda\gamma$ invariant mass and Σ^0 momentum is equal to 3.5 MeV/c^2 and 6 MeV/c, respectively.

The minimum momentum for the proton tracks is varied within 10 MeV/c of the central value of 170 MeV/c. Variations of 15% are tested for the time windows used to select the machine background, the photon signal and π^0 background selection independently. As for the machine background subtraction, the systematic error is evaluated by repeating the fit allowing variations within 1σ of the initial Σ^0 mass fit parameters. For what concerns the simulated distributions, the systematic errors are also evaluated for the minimum momentum of the nucleons required to exit the nucleus in the absorption simulation and the probability of having more than one collision when simulating the FSI with the residual nucleus following a 2NA process.

The minimum momentum for the nucleons is sampled according to the Fermi momentum distribution between 170 and 220 MeV/c. The systematic error is evaluated by varying the two boundaries by 15% in both directions. For the systematic variation of the probability of having one or two collisions for the FSI process two cases, 40/60% and 60/40%, are evaluated respectively.

The final fit results deliver the contribution of the different channels to the analysed $\Sigma^0 p$ final state. The best fit delivers a χ^2/ndf of 0.85. The emission rates extracted from the fit are normalised to the total number of stopped antikaons, as summarised in Table 1. The fit results lead to the first measurements of the genuine 2NA-QF for the final state $\Sigma^0 p$ in reactions of stopped K$^-$ on targets of ^{12}C and ^{27}Al. This contribution is found to be only 9% of the total absorption cross-section including 2NA, 3NA and 4NA processes with also the contribution of the uncorrelated background leading to a $\Sigma^0 p$ final state taken into account.

Table 1

Production probability of the $\Sigma^0 p$ final state for different intermediate processes normalised to the number of stopped K$^-$ in the DC wall. The statistical and systematic errors are shown as well. "Tot 2NA" stands for the sum of the 2NA-QF and the 2NA-FSI processes. "Tot 3 body" stands for the sum of 2NA-FSI and 3NA processes.

	yield/K$^-_{stop} \cdot 10^{-2}$	$\sigma_{stat} \cdot 10^{-2}$	$\sigma_{syst} \cdot 10^{-2}$
2NA-QF	0.127	±0.019	$^{+0.004}_{-0.008}$
2NA-FSI	0.272	±0.028	$^{+0.022}_{-0.023}$
Tot 2NA	0.399	±0.033	$^{+0.023}_{-0.032}$
3NA	0.274	±0.069	$^{+0.044}_{-0.021}$
Tot 3 body	0.546	±0.074	$^{+0.048}_{-0.033}$
4NA + bkg.	0.773	±0.053	$^{+0.025}_{-0.076}$

Similar measurements have been carried out and reported in [9,20]. In [9] stopped K$^-$ in a ^{4}He target have been considered and the integrated contribution to the final state $\Sigma^0(\Lambda)$ with no pion emission was extracted and found to be equal to 0.117 ± 0.024 per stopped K$^-$. This large number is due to the Λ contamination in the sample and to the fact that absorptions on p-n pairs are included. The data in [20] show the measurement of the $\Sigma^- p$ final state from a ^{13}C target. There, a yield of $0.46 \pm 0.09(\text{stat}) \pm 0.02(\text{syst}) \cdot 10^{-2}$ per stopped K$^-$ is attributed to the K$^-$ absorption on a p-n pair.

Even if the employed simulation model is rather simplified, the treatment of 2NA-QF is satisfactory for our purpose and the signature of this component well distinguishable from the other contributions, especially in the $\Sigma^0 p$ invariant mass distribution. On the other hand, a clear disentanglement of the 3NA process from the 2NA followed by FSI is difficult, due to the overlap of the relevant kinematic variables over a wide range of the phase space.
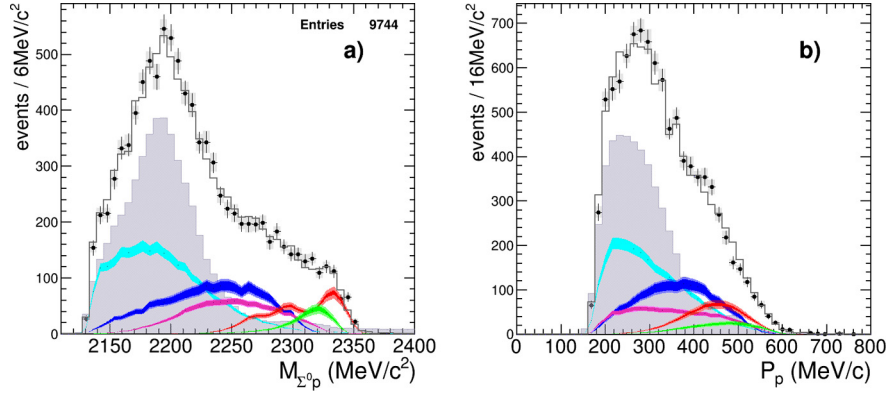
Fig. 3. (Colour online.) Σ^0p invariant mass and proton momentum distributions together with the results of the global fit including the ppK$^-$. The different contributions are labeled as in Fig. 2 and the green histograms represent the ppK$^-$ signal.

Two tests were performed that demonstrate that both physical processes should be included in the fit. First, if the 3NA contribution is switched off a variation of the reduced χ^2 of 0.19 from 0.85 (the best fit) to 1.05 is observed. Such effect is mainly due to the fact that the Σ^0 and the proton momentum distributions are no longer well described. The other kinematic distributions are less sensitive to this contribution. In particular, the χ^2 calculated for the fit result of the proton momentum distribution only is deteriorated by 47% when excluding the 3NA contribution from the fit. As a second limiting case the 2NA + FSI contribution was discarded, leading to a reduced χ^2 of 1.18. In this case the $\cos(\theta_{\Sigma^0 p})$ and Σ^0p invariant mass distributions are not properly reproduced.

The uncorrelated emission of the Σ^0p is also not distinguishable from the 4NA process and hence these two contributions are added up.

4. Search for the ppK$^-$ bound state signal

The last step of the analysis consists in the search of the ppK$^-$ bound state produced in K$^-$ interactions with nuclear targets, decaying into a Σ^0p pair. The ppK$^-$ are simulated similarly to the 2NA-QF process but sampling the mass of the ppK$^-$ state with a Breit–Wigner distribution, rather than the Fermi momenta of the two nucleons in the initial state. The event kinematic is implemented by imposing the momentum conservation of the ppK$^-$-residual nucleus system. Different values for the binding energy and width varying within 15–75 MeV/c^2 and 30–70 MeV/c^2 in steps of 15 and 20 MeV/c^2, respectively, are tested. This range is selected according to theoretical predictions [14] and taking into account the experimental resolution. The global fit is repeated adding the ppK$^-$ state to the processes 1–4. The best fit (χ^2/ndf = 0.807) is obtained for a ppK$^-$ candidate with a binding energy of 45 MeV/c^2 and a width of 30 MeV/c^2, respectively. Fig. 3 shows the results of the best fit for the Σ^0p invariant mass and proton momentum distributions where the ppK$^-$ bound state contribution is shown in green. The resulting yield normalised to the number of stopped K$^-$ is ppK$^-$/K$^-_{stop}$ = $(0.044 \pm 0.009stat^{+0.004}_{-0.005}syst) \cdot 10^{-2}$. Fig. 4 shows the yield results from the two best fits of the bound state with a width of 30 MeV/c^2 and a binding energy of 45 and 60 MeV/c^2, respectively, with statistical errors calculated by MINOS at 1σ (black line), 2σ (blue boxes) and 3σ (red boxes). The inclusion of the ppK$^-$ bound state to the global fit introduces an additional parameter and this improves the fit quality. Considering also that the improvement of the χ^2 is only marginal, an F-Test is carried out to compare the two models: with and without ppK$^-$ bound state. This test consists in evaluating the statistical significance of the model with the ppK$^-$, accounting for the ad-
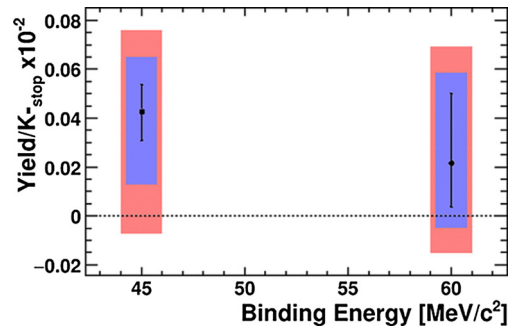

Fig. 4. (Colour online.) ppK$^-$ yield normalised to the number of stopped K$^-$ for the two best fits corresponding to binding energies of 45 and 60 MeV/c^2 and width of 30 MeV/c^2 for the ppK$^-$ bound state. The errors are only statistical calculated by MINOS at 1 (black line), 2 (blue boxes) and 3 (red boxes) σ.
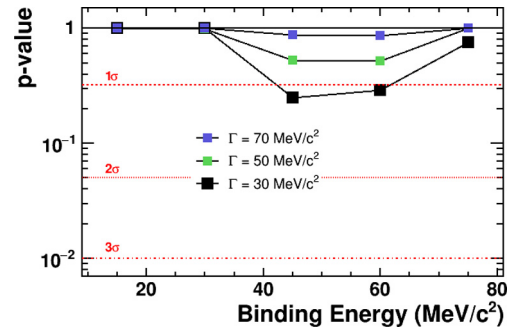

Fig. 5. (Colour online.) p-Value resulting from the F-test that compares the two fitting hypotheses. Horizontal lines showing up to 3σ are drawn.

ditional fit parameter, by comparing the residuals and number of degrees of freedom of two models. The resulting F value reads as follows:

$$F = \frac{(SSE_1 - SSE_2)/(ndf_1 - ndf_2)}{SSE_2/ndf_2} \tag{1}$$

with SSE being the quadratic sum of the residuals bin per bin and ndf the number of degrees of freedom of each model. The global p-value associated to the obtained F value and from the number of parameters in each model is shown in Fig. 5 for bound state simulations with a width of 30, 50 and 70 MeV/c^2 as a function of the binding energy. One can see that even the best fit corresponds to a p-value equal to 0.25 and hence to a significance of 1 σ.

This implies that although the fit favours the presence of an additional component that can be parametrised with a Breit–Wigner

distribution with a certain mass and width, its significance is not sufficient to claim the observation of the bound state. The present data lacks of sensitivity for investigating the existence of a bound state with a larger binding energy and/or width than those considered in the described analysis.

5. Summary

We have presented the analysis of the K^- absorption processes leading to the $\Sigma^0 p$ final state measured with the KLOE detector. It is shown that the full kinematics of this final state can be reconstructed and a global fit of the kinematic variables allows to pin down quantitatively the different contributing processes. A cocktail of processes including simulations of the K^- absorption on two or more nucleons with or without final state interactions and background processes estimated with experimental data is used for the global fit. The absorption on two nucleons without final state interaction (2NA-QF) is isolated and the yield normalised to the number of absorbed K^- is presented in this work for the first time. It is shown that it is difficult to distinguish between the case where K^- are absorbed on three nucleons (3NA) or when the two-nucleon absorption is followed by a final state interaction (2NA-FSI). For this purpose the data should be further interpreted with the help of theoretical calculations. The 2NA-QF yield is found to be about 20% of the sum of the 3NA and 2NA-FSI processes. If one considers the ratio of the 2NA-QF to all other simulated processes a value of about 9% is obtained. Hence, we conclude that the contribution of the 2NA-QF processes for K^- momenta lower than 120 MeV/c is much smaller in comparison with other processes.

A second fit of the experimental data including the contribution of a ppK$^-$ bound state decaying into a $\Sigma^0 p$ final state is carried out. A systematic scan of possible binding energies and widths varying within 15–75 MeV/c^2 and 30–70 MeV/c^2, respectively, is performed and the best value of the total reduced χ^2 is achieved for the hypothesis of a ppK$^-$ with a binding energy of 45 MeV/c^2 and a width of 30 MeV/c^2. The corresponding ppK$^-$ yield extracted from the fit is ppK$^-$/K$^-_{stop} = (0.044 \pm 0.009 stat^{+0.004}_{-0.005} syst) \cdot 10^{-2}$. An F-test is conducted to compare the simulation models with and without the ppK$^-$ signal and to extract the significance of the result. A significance of only 1 σ is obtained for the ppK$^-$ yield result. This shows that although the measured spectra are compatible with the hypothesis of a contribution of the channel $ppK^- \rightarrow$ $\Sigma^0 + p$, the significance of the result is not sufficient to claim the observation of this state.

Acknowledgements

References

[1] D. Cabrera, et al., Phys. Rev. C 90 (2014) 0552017.
[2] A.E. Nelson, D.B. Kaplan, Phys. Lett. B 192 (1987) 193.
[3] C. Fuchs, Prog. Part. Nucl. Phys. 56 (2006) 1, nucl-th/0507017.
[4] M. Bazzi, et al., SIDDHARTA Coll., Phys. Lett. B 704 (2011) 113.
[5] P. Demorest, et al., Nature 467 (2010) 1081;
    F. Özel, et al., Astrophys. J. 757 (2012) 55.
[6] D. Gazda, E. Friedman, A. Gal, J. Mares, Phys. Rev. C 77 (2008) 045206.
[7] A. Forster, et al., Phys. Rev. Lett. 91 (2003) 152301;
    P. Crochet, et al., Phys. Lett. B 486 (2000) 6;
    G. Agakishiev, et al., Phys. Rev. C 82 (2010) 044907.
[8] V. Zinyuk, et al., FOPI Coll., Phys. Rev. C 90 (2014) 025210.
[9] P.A. Katz, et al., Phys. Rev. D 1 (1970) 1267.
[10] T. Suzuki, et al., Mod. Phys. Lett. A 23 (2008) 2520.
[11] A. Gal, Nucl. Phys. A 914 (2013) 270.
[12] N. Kaiser, P.B. Siegel, W. Weise, Nucl. Phys. A 594 (1995) 325;
    E. Oset, A. Ramos, Nucl. Phys. A 635 (1998) 99;
    B. Borasoy, U.G. Meißner, R. Nißler, Phys. Rev. C 74 (2006) 055201;
    T. Hyodo, W. Weise, Phys. Rev. C 77 (2008) 035204.
[13] R.J. Hemingway, Nucl. Phys. B 253 (1985) 742, CERN-EP/84-113;
    I. Zychor, et al., ANKE Coll., Phys. Lett. B 660 (2008) 167;
    G. Agakishiev, et al., HADES Coll., Phys. Rev. C 87 (2013) 025201;
    K. Moriya, et al., Phys. Rev. C 87 (2013) 3.
[14] T. Yamazaki, Y. Akaishi, Phys. Rev. C 76 (2007) 045201;
    A. Doté, T. Hyodo, W. Weise, Phys. Rev. C 79 (2009) 014003;
    S. Wycech, A.M. Green, Phys. Rev. C 79 (2009) 014001;
    N. Barnea, A. Gal, E.Z. Liverts, Phys. Lett. B 712 (2012) 132;
    N.V. Shevchenko, A. Gal, J. Mares, Phys. Rev. Lett. 98 (2007) 082301;
    Y. Ikeda, T. Sato, Phys. Rev. C 79 (2009) 035201;
    E. Oset, et al., Nucl. Phys. A 881 (2012) 127.
[15] M. Agnello, et al., FINUDA Coll., Phys. Rev. Lett. 94 (2005) 212303;
    T. Yamazaki, et al., Phys. Rev. Lett. 104 (2010) 132502;
    G. Agakishiev, et al., HADES Coll., Phys. Lett. B 742 (2015) 242;
    Y. Ichikawa, et al., Prog. Theor. Exp. Phys. 021D01 (2015).
[16] F. Bossi, et al., Riv. Nuovo Cimento 31 (10) (2008).
[17] A. Gallo, et al., Conf. Proc. C060626 (2006) 604.
[18] K.A. Olive, et al., Particle Data Group, Chin. Phys. C 38 (2014) 090001.
[19] V.K. Magas, E. Oset, A. Ramos, Phys. Rev. C 74 (2006) 025206.
[20] M. Agnello, et al., Phys. Rev. C 92 (2015) 045204.